https://dx.doi.org/10.1016/j.enconman.2022.116047

Indirect evaporative cooling maps of China: Optimal and quick performance identification based on a data-driven model

Wenchao Shi [a,*], Xiaochen Ma [a], Yu Gu [b], Yunran Min [c], Yi Chen [c], Hongxing Yang [a,*]

[a] Renewable Energy Research Group (RERG), Department of Building Environment and Energy Engineering, The Hong Kong Polytechnic University, Hong Kong, China

[b] Department of Urban Informatics, School of Architecture and urban planning, Shenzhen University, Guangdong, China

[c] School of Mechanical and Energy Engineering, Jimei University, Fujian, China

Abstract

The data-driven models of various air conditioning (AC) systems have been developed because of the wider application of machine learning in the engineering field. Indirect evaporative cooler (IEC), known as one of the effective and environment-friendly AC devices, achieves the cooling purpose without using any types of mechanical compressors or chemical refrigerants. Recent studies on various IECs have been carried out in full swing with a large amount of valuable data produced. However, the data-driven model of the cross-flow IEC for sensible cooling and total cooling is yet to be developed. In addition, by extracting the indoor cold exhaust air into the secondary air channel, the application range of an IEC can be extended, but so far the performance of IEC used in different regions has been rarely evaluated. In this study, a IEC model was established based on the artificial neural network (ANN), which was validated with the on-site measurement results from a real engineering project. Combining the selected geometric size of IEC and various outdoor weather conditions into the IEC-ANN model, a case study was conducted to present the annual and seasonal IEC performance maps of China, and the optimal application regions could be determined. Results show that south China, east China, and middle China are more suitable to employ IEC for air treatment. The greatest average temperature drop and cooling capacity are obtained in south China with 4.52 ℃ and 5.74 kW, respectively. In addition, the inference time of this IEC-ANN model was significantly shorter compared with that of a numerical model, indicating the good potential of improving the work efficiency when it is used for forecasting the performance of IEC in the design stage of a practical project.

Keywords

Air conditioning; Indirect evaporative cooling; Data-driven model; Cooling map; Optimal and quick identification

* Corresponding author.
E-mail addresses: wenchao511.shi@connect.polyu.hk (W. Shi), hong-xing.yang@polyu.edu.hk (H. Yang).

Nomenclature

a	Neurons in hidden layers	***Abbreviations***	
c_{pa}	Specific heat of air, J/(kg ·℃)		
c_{pw}	Specific heat of water, J/(kg ·℃)	1-D	One-dimensional
D	External width, mm	2-D	Two-dimensional
d_e	hydraulic diameter of channel, m	3-D	Three-dimensional
H	Height, mm	AC	Air conditioning
H	Height, m	ANN	Artificial neural network
h	Heat transfer coefficient, W/(m^2 · ℃)	COP	Coefficient of performance
h_m	Mass transfer coefficient, kg/(m^2 · s)	IEC	Indirect evaporative cooler
i	Enthalpy, kJ/kg	R^2	Coefficient of correlation
L	Length, mm	RH	Relative humidity
Le	Lewis number	*RMSE*	Root mean square error
m	mass flow rate of air, kg/s		
N	Number of channel pairs		
n	Number of neurons	***Subscripts***	
Nu	Nusselt number	c	Condensation
Pr	Prandtl number	e	Evaporation
Q	Cooling capacity, W	in	Inlet
Re	Reynolds number	out	Outlet
s	Channel gap distance, mm	p	Primary air
t	Temperature, ℃	pre	Precool by IEC
v	Velocity, m/s	s	Secondary air
w	Humidity, g/kg	w	Water film
W	Weight	wb	Wet-bulb
X	Neurons in the input layer	t_w	Water temperature
Y	Neurons in the output layer		
Greek symbols			
λ	Thermal conductivity W/(m · ℃)		
θ	Bias		

1. Introduction

Relying on the power-intensive compressor and a variety of refrigerants, the traditional vapor-compression air conditioning (AC) system is employed to handle the cooling load of the indoor environment, which consumes excessive energy with the growing demand of thermal comfort. To ease the intensive electricity usage in buildings, sustainable AC technologies are increasingly studied. For instance, the indirect evaporative cooler (IEC), taking away the heat through the physical evaporation process, is regarded as one of the reliable approaches. Fig. 1 displays the essential components in an IEC system, including the main cooler, two fans, the water pump, nozzles, and connection accessories. For the main cooler, two adjacent channels are named as a primary air (supply air) channel and a secondary air (working air) channel. Water is only sprayed to the secondary air channel surface to develop the thin water film, and it will evaporate owing to the humidity gradient when the air is passing [1].

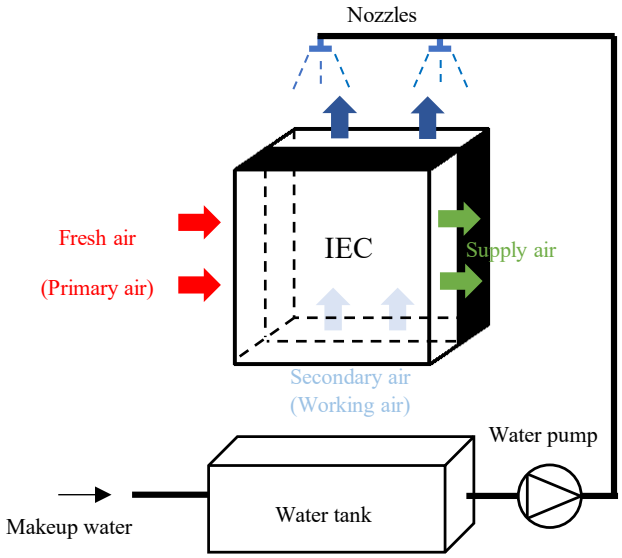

Fig. 1 Basic structure of a cross flow IEC system

Researchers have carried out comprehensive studies on the IEC modelings and experiments. Boukhanouf et al. developed a counter-flow numerical IEC model under hot-arid and climate regions, which achieved up to 1.02 wet-bulb efficiency and partially substituted conventional system for air cooling [2]. Jia et al. put forward a counter-cross flow IEC made of hexagon polystyrene sheets. This structure could handle an increasing volume of supply air compared with normal IECs, and the dew point efficiency and COP reached up to 0.71 and 13.8, respectively [3]. Utilizing the indoor return air or part of the primary air as secondary air, a counter-flow IEC model was proposed to precool the fresh air in hot-humid regions, which contained the cooling and dehumidification effects [4]. A cross-flow IEC model considering the influence of wettability of secondary air channel was established, indicating the wet-bulb efficiency increased from 0.63 to 0.92 when the wetting ratio grew from 0.5 to 1 [5]. Some two-dimensional (2-D) or three-dimensional (3-D) models were developed by applying the

computational fluid dynamics (CFD) approach. 2-D models could reveal the temperature variations in IECs with different airflow arrangements [6], and the 3-D model took the gradient on the channel height into account; thus, the prediction accuracy was improved by 5.8% compared with the previous one [7].

In addition to the normal IEC, efforts were made to some novel internal shapes and channel surface materials. The effect of condensation, due to the high inlet air humidity, generated on the IEC heat transfer plate was inspected. Min et al. compared the bare aluminum IEC sheet and the sheet with hydrophobic coating. Results showed that the energy saving ratio was enhanced by 8.5 to 17.2 % because of the accelerated depature of condensate [8]. Kabeel et al. investigated the IEC with baffles inside the supply air channel, and the outlet temperature declined by more than 15% with the growing number of baffles [9]. Shi et al. developed a dynamic model of IEC sintered porous material on the secondary air channel walls (PIEC) to absorb sprayed water [10]. The feasibility of the periodic spraying was proved by experiments, which realized to reduce more than 90% operational energy cost [11]. Artificial plant fiber-polymer, with advantages of low price and light weight, was made as evaporative material for a counter flow IEC, and the most significant energy efficiency ratio was measured as 11.0 [12].

Referring to the existing IEC research, it was noticed that the existing models were built based on heat and mass transfer theories, and massive valuable data was collected during the process. Most of the data were used to analyze the effects of essential parameters such as air temperature, relative humidity, and velocity on the cooling performance. However, with the increasing popularity of machine learning in recent years, the generated simulation results or experimental data has the potential to be furtherly employed to develop models for prediction purposes, and this approach has been generally found in some AC systems. For instance, Jani et al. assessed the desiccant wheel in a hybrid AC system by an artificial neural network (ANN) model trained by experimental data. The model was proved to work out the dehumidification rate in various inlet conditions in acceptable discrepancies [13]. Zhu et al. discussed an ANN model of counter flow IEC used in hot and dry regions based on results from a 1-D numerical model. A comprehensive parametric analysis was conducted, and the optimal range of the extraction air ratio was decided from 0.3 to 0.36 [14]. Li et al. trained several machine learning models of the photovoltaic air conditioner by utilizing simulation results from Energyplus software, and the extreme gradient boosting model could achieve the optimal accuracy for the indoor environment [15]. Ohno et al. proposed a Bayesian ANN model of a direct expansion AC system using reliable simulation data, and the dynamic variations of room temperatures and exergy destructions were identified. The results could guide the operation control strategies to meet the required thermal comfort with minor exergy loss [16]. In a hybrid ejector AC system, the ANN model was to forecast the reliable outlet values of each component. The multi-layer perceptron (MLP) was selected as the most suitable neural network compared with the other two types, radial basis function (RBF) and support vector machine (SVM) [17]. Mohammad et

al. adopted single and multi-layer ANNs to estimate the effectiveness of a desiccant generator in a solar-assist AC system, and the minimum prediction deviations of temperature and moisture content were only 1.4 ℃ and 2.1 g/kg compared with the true measured values [18]. Xu et al. examined the ground source heat pump system with an ANN model, which indicated that higher soil thermal conductivity, deeper vertical well, narrower well diameter, and larger water flow rate could improve the heat transfer capacity [19].

Referring to the above review of published studies, there are still pieces of research gaps that can be recognized as follows. Firstly, the data-driven model of the cross flow IEC is rarely built, although plenty of numerical models and real tests were implemented. Secondly, the existing research usually analyzed the IEC under a specific weather feature. Utilizing the exhaust air from indoor air-conditioned areas, the application regions of IEC can be extended. However, studies on the performances of IEC under various weather conditions of different seasons in the national range were limited. Thirdly, the more applicable areas of the IEC were yet to be determined. Fourthly, the comparison of the prediction efficiency between the ANN model and the traditional IEC numerical model are scarcely conducted.

In this paper, the ANN model of cross flow IEC using the cool indoor air as secondary air was established, which was verified by the on-site measurement results of a real IEC project. Then, combining with the climate conditions in a variety of cities, the IEC cooling performance maps of China were made, and the optimal regions to use IEC were presented as well. Finally, the short inference time of this model was illustrated and compared with it of a numerical model, which can improve the work efficiency when it is employed for predicting the performance in the engineering project.

2. Model establishment and validation

2.1 Description of numerical IEC model

The 2-D numerical model of the cross flow IEC for sensible cooling (without dehumidification in dry climate regions) and total cooling (with dehumidification in humid weather areas) has been established according to the general assumptions in our previous study [20, 21], and the critical equations were briefly depicted as follows.

For the secondary air, the heat and mass transfer equations between water film and air can be written from Eq. (1) to Eq. (3):

$$h_s(t_w - t_s) \cdot dxdy + h_{fg} h_{ms}(\omega_{t_w} - \omega_s) dxdy = \dot{m}_s \frac{\partial i_s}{\partial y} dy \tag{1}$$

$$h_{ms}(\omega_{t_w} - \omega_s) \cdot dxdy = m_s \frac{\partial \omega_s}{\partial y} \cdot dy \tag{2}$$

$$\dot{m}_s = \frac{dx}{L} m_s \tag{3}$$

For the primary air, the heat transfer equation under the non-condensation state is:

$$h_p(t_p - t_w) \cdot dxdy = c_{pa}\dot{m}_p \frac{\partial t_p}{\partial y} dx \tag{4}$$

$$\dot{m}_p = \frac{dy}{H} m_p \tag{5}$$

When the IEC treats the air in dry climate regions, no dehumidification is going to occur, thus the energy balance is expressed as:

$$\dot{m}_s \frac{\partial i_s}{\partial y} - c_{pa}\dot{m}_p \frac{\partial t_p}{\partial x} = \quad c_{pw} t_{ew} \frac{\partial m_e}{\partial y} \tag{6}$$

$$\frac{\partial m_e}{\partial y} = \dot{m}_s \frac{\partial w_s}{\partial y} \tag{7}$$

The convective heat and mass transfer coefficients are bridged by Lewis number as Eq. (8) [22]. The convective heat transfer coefficient is related to the Nusselt number Eq. (9), and the Nusselt number can be calculated by Eq. (10) [2].

$$Le^{\frac{2}{3}} = \frac{h_s}{h_{ms} c_{pa}} \tag{8}$$

$$h = \frac{Nu \cdot \lambda}{d_e} \tag{9}$$

$$Nu = 0.664 Re^{\frac{1}{2}} Pr^{\frac{1}{3}} \tag{10}$$

When the IEC handles hot and humid air such as in Hong Kong, it removes both sensible and latent load if the secondary air is from the cool indoor space. Hence, the mass transfer equation in the primary air channel is written as Eq. (11), and the latent heat is released simultaneously. Accordingly, the energy balance equation should be modified into Eq. (13):

$$h_{mp}(\omega_p - \omega_w) \cdot dxdy = \dot{m}_p \frac{\partial \omega_p}{\partial x} \cdot dx \tag{11}$$

$$-\dot{m}_p \frac{\partial \omega_p}{\partial x} = \frac{\partial m_c}{\partial y} \tag{12}$$

$$\dot{m}_s \frac{\partial i_s}{\partial y} - \dot{m}_p \frac{\partial i_p}{\partial x} = c_{pw} t_{ew} \frac{\partial (m_e)}{\partial y} + c_{pw} t_{cw} \frac{\partial (m_c)}{\partial y} \tag{13}$$

The finite difference method was adopted to discretize the above sets of partial differential equations for each element into the algebraic equations. The boundary conditions and detailed

solving and validating process of this numerical model can be found in our previous work of Ref. [20], which were programmed in MATLAB platform. Then, the results of this model were devoted to establishing the IEC-ANN model, which was introduced in the following sub-section.

2.2 IEC-ANN model development

2.2.1 Basic introduction of the ANN

The ANN model can fit the nonlinear relationship between input and output based on the massive data. Multi-layer perception (MLP), which is regarded as the most common and efficient type of ANN in the research area of AC systems, consists of an input layer, multiple hidden layers, and an output layer [23], which was also adopted in this study.

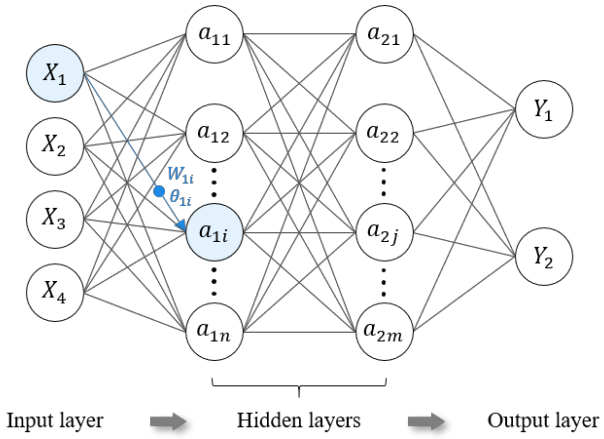

Fig. 2 Structure of the multi-layer perception

A typical MLP structure is shown in Fig. 2. There are four dimensions of X_1~X_4 as the input data. In the first place, the elements of input layer are computed via nonlinear transformation into new values in the first hidden layer. For instance, in the neuron a_{1i} of the first hidden layer, input element X_1 is transformed to a_{1i} based on Eq. (14). W_{1i} and θ_{1i} donote the weight and bias of a_{1i} respectively, and f is the activation function [24].

$$a_{1i} = f\left(\sum_{i\in(1,n)} X_1 \times W_{1i} + \theta_{1i}\right) \tag{14}$$

In this IEC-ANN model, the Sigmoid function is decided as the activation function, which is written in Eq. (15) [25]:

$$f(x) = \frac{1}{1+e^{-x}} \tag{15}$$

The hidden layers can achieve linear computation with weight and bias as well as the non-linear with activation function. Therefore, the ANN holds a fitting ability for the complicated relationship between input and output. Finally, after these hidden layers, output layer could

figure out the required output Y_1 and Y_2.

It can be realized that the model performance is influenced by the unknown weight and bias in layers. In order to obtain the optimal weight and bias, the ANN model is trained through Back Propagation (BP). A loss function is used to evaluate the model performance according to the deviation between the predicted and true values during BP. In this study, root mean square error (*RMSE*) is used as the loss function, which is expressed by Eq. (16). Afterward, the unknown weights and bias are going to be updated through the Gradient Descent algorithm constantly until the loss function achieves convergence.

$$RMSE = \sqrt{\frac{\sum_{i=1}^{n}(x_{i,predict} - x_{i,true})^2}{n}} \tag{16}$$

2.2.2 Introduction of the data sets and model settings

The influential parameters of IEC have been determined based on the published studies [20, 21], which contain the inlet air temperature, RH, velocity of primary and secondary air, the channel height, and the length/height of the IEC sheet. The common ranges of these parameters are listed in Table 1. Typically, the shape of the IEC sheet is square, therefore the length and height are the same, and only one value of the two is needed. In addition, the heights of primary air and secondary air channels are usually equal in practice situations. A group of input data includes nine variables, and there are 21184 groups of data in total input for establishing the IEC-ANN model.

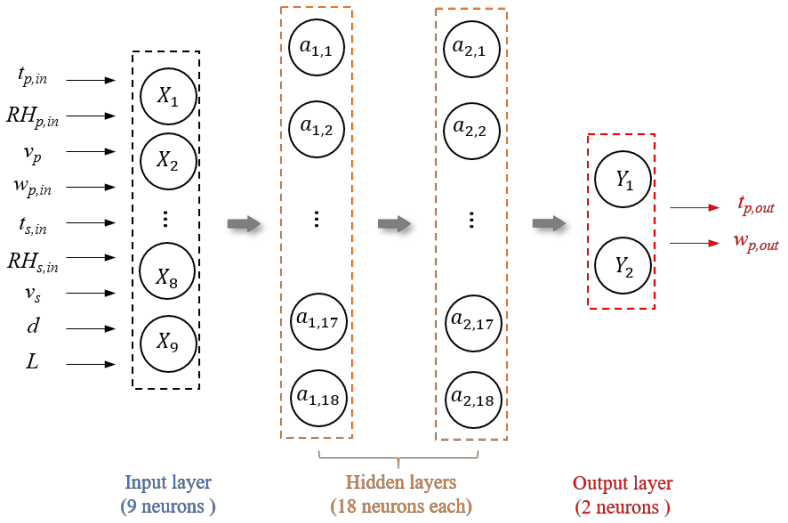

Fig. 3 The structure of the multi-layer IEC-ANN model

Considering the current data dimensions and scales, 2 hidden layers with 18 neurons each were capable of fitting the relationship between the input and output variables. The ultimate format of this IEC-ANN model structure was exhibited in Fig. 3, which is programmed in MATLAB software. The data set was divided into three parts as training, validation, and test data sets with the proportions of 70%, 15%, and 15%, respectively. The learning rate and epoch were set as 0.001 and 3000.

Table 1 Summary of input conditions of the cross flow IEC

Parameter	Range	Parameter	Range
t_p (℃)	[20, 2, 36]	t_s (℃)	[21, 1, 23]
RH_p (%)	[20, 5, 95]	RH_s (%)	[50, 10, 80]
v_p (m/s)	[1.5, 0.5, 3]	v_s (m/s)	[1, 0.5, 2]
s (mm)	[0.004,0.001,0.006]	L (m)	[0.4, 0.2, 1]

[a_1, i, a_2]: a_1: start value; i: interval; a_2: end value

2.2.3 Performance of the IEC-ANN model

Basically, there are two commonly-used indicators, namely, *RMSE* and coefficient of determination (R^2), were employed to evaluate the performance of the trained model using test data, which are formulated by Eq. (16) and Eq. (17) [26]. It needs to be mentioned that the purpose of *RMSE* is different from it in the previous section. In this section, this *RMSE* is used to evaluate the prediction performance during the test procedure, while this indicator is a signal of finishing the training process based on the convergence in section 2.2.1. R^2 can examine the fitting degree of the model, where the result of 1 demonstrates a perfect fit, and it means a reliable model for predictions. After model testing, the values of *RMSE* and R^2 are calculated as 0.603 ℃ and 0.936 for the primary air outlet temperature, while the values of them are 0.327 g/kg and 0.996 for the primary air outlet humidity, which both show good performances of this IEC-ANN model.

$$R^2 = 1 - \frac{\sum_{i=1}^{n}(x_{predict} - x_{i,real})^2}{\sum_{i=1}^{n}(x_{i,real} - x_{i,real,ave})^2} \quad (17)$$

2.3 On-site measurement validation

2.3.1 Project description

In order to validate that this IEC-ANN model can achieve an acceptable prediction accuracy in practice, the on-site measurement was conducted in a project. The project was arranged on the 10th floor of a logistics center in Hong Kong. The hybrid IEC system with sensor positions is briefly depicted in Fig. 4. Generally, the fresh air was handled by the IEC unit combined with an axillary coil section, which was supplied to the indoor office area. The outdoor air was firstly precooled by IEC, and the remaining cooling load was treated by the coil. Based on the outlet temperature of the coil, the electric valve installed on the chilled water pipe would control the water flowrate to make the final air temperature approach the required supply temperature. It needs to be mentioned that the primary and secondary air sources of a traditional IEC are both outdoor air. However, in order to achieve a greater cooling effect, the secondary air source was the exhaust air from the indoor air-conditioned space in this project, because it has a lower wet-bulb temperature than using the hot and humid outdoor fresh air, and the fluctuations of the indoor cool air properties were less than them of outdoor area, which made the cooling effect more stable. The essential specifications of the IEC, coil and operating

information were summarized in Table 2.

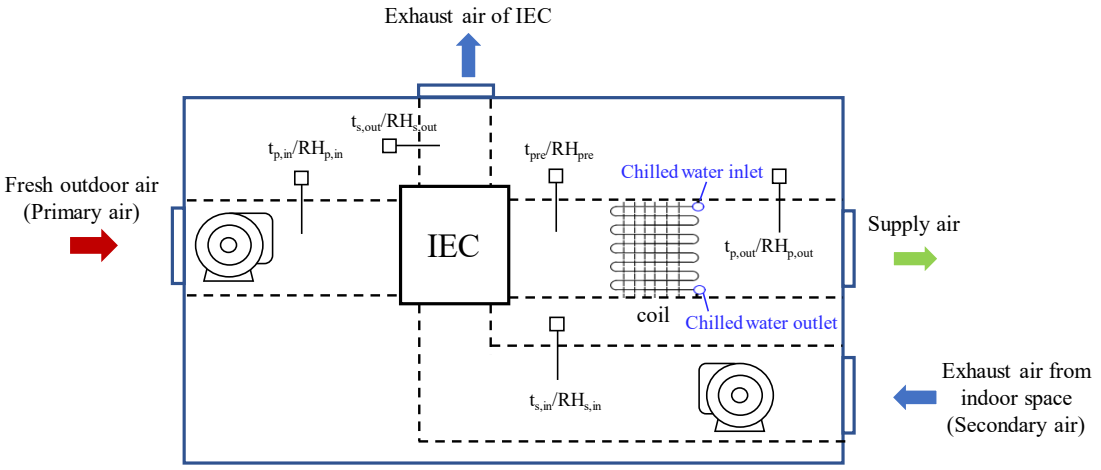

Fig. 4 Schematic diagram of the hybrid IEC system

Table 2 Summary of basic project information

Device	Parameter	Value	Parameter	Value
IEC	H (m)	0.6	L (m)	0.6
	D (m)	0.8	s (mm)	4
	v_p (m/s)	2.5~3	v_s (m/s)	0.5~1
	N (pair)	90		
	Air source: Primary air - Outdoor door; Secondary air- indoor exhaust air			
Cooling coil	Rows of tube	4	Fins per inch (FPI)	12
	Fin thickness (mm)	0.12	Tube diameter (OD)	3/8"
	Tube thickness (mm)	0.35	Total capacity (kW)	44.51
	Sensible/total capacity ratio	0.38	Water flow rate (L/s)	2.13
	Length (mm)	400	Height (mm)	812
	Operating time: 8.00 a.m. to 6.00 p.m.			

2.3.2 Comparison between predicted values and on-site measurement data

Fig. 5 shows the variations of the local outdoor air properties of the logistics center during the operation period. The outlet air temperature and humidity of the IEC measured from the related transmitters in the system were compared with the predicted values from this IEC-ANN model and the numerical model in Fig. 6. It can be observed that the prediction results have a good agreement with the real data. The maximum discrepancies of temperatures between the measured data and predictions were 3.2% and 4.1%, and the biggest deviation of humidity values were 7.3% and 6.3% for the IEC-ANN model and the numerical model, respectively, which were acceptable and could validate that this IEC-ANN model was capable of forecasting the performance of IEC in the real situations of the engineering project.

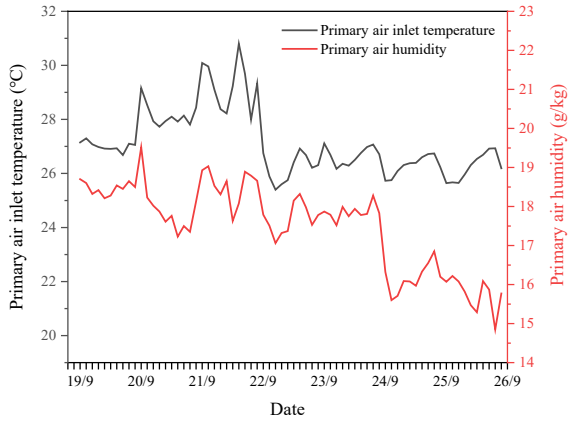

Fig. 5 The primary temperature and humidity during the test period

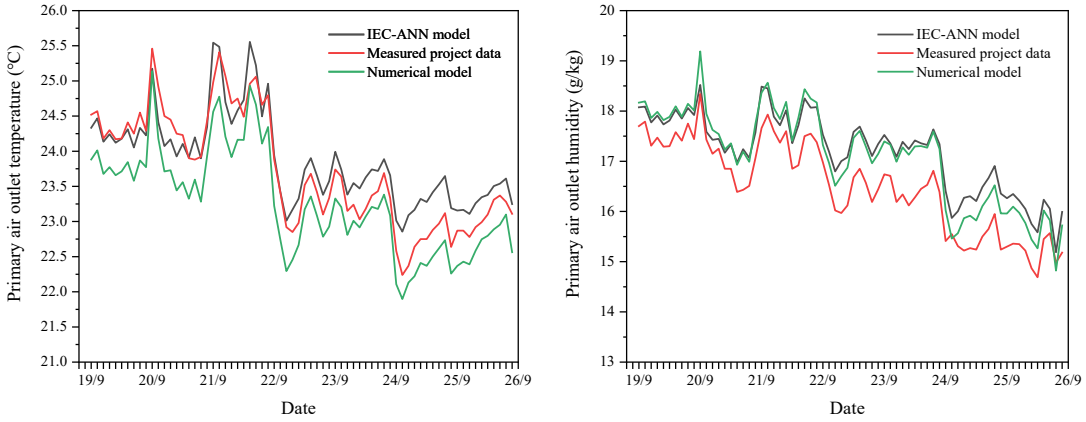

(a) Temperature (b) Humidity

Fig. 6 Comparison between the real data and predicted values from the IEC-ANN model and the numerical model

3. Results and discussions

In order to quantitively reflect the performance of cross flow IEC by the ANN model, a case study on assessing the cooling potential was conducted based on the geometric and operating conditions of H = 0.6 m; L = 0.6 m; s = 0.004 m; N = 100 pairs; v_p = 2.5 m/s; v_s = 1 m/s. As illustrated in section 2.3.1, using the indoor exhaust cool air as the secondary air can not only achieve a larger air temperature decrease, but expand the application region of IEC that traditionally is limited by the weather conditions when the secondary air is from outdoor space. In this section, the indoor cool exhaust air used for secondary air can be set as 23 ℃ and 60% [27]. Fig. 7 shows the division of seven geographical regions of China. The outdoor weather information used in this study originates from the online EnergyPlus weather database [28], and the seasonal maps of the average temperature and RH can be found in Appendix 1. In addition, it is also known that the four seasons and their corresponding months are spring (from March to May), summer (from June to August), autumn (from September to November), and winter (from December to February of next year) in China.

Given the above conditions in the IEC-ANN model, the annual average performance and

average seasonal performance of IEC in the working period and the non-working period were determined, and the optimal regions to use IEC were able to be identified. It needs to be mentioned that the two periods of a day were divided according to the working time of people in the real situation, which were set as 8:00 a.m. to 6:00 p.m. for the working/daytime period and 6:00 p.m. to 8:00 a.m. for the non-working/nighttime or rest period in this study. Furthermore, the comparison of the inference time between the numerical IEC model and this IEC-ANN model was exhibited in section 3.3, which would indicate that the IEC-ANN model was suitable for improving the work efficiency in the engineering stage.

Fig. 7 Division of seven geographical regions of China [29]

3.1 Annual average performance of IEC

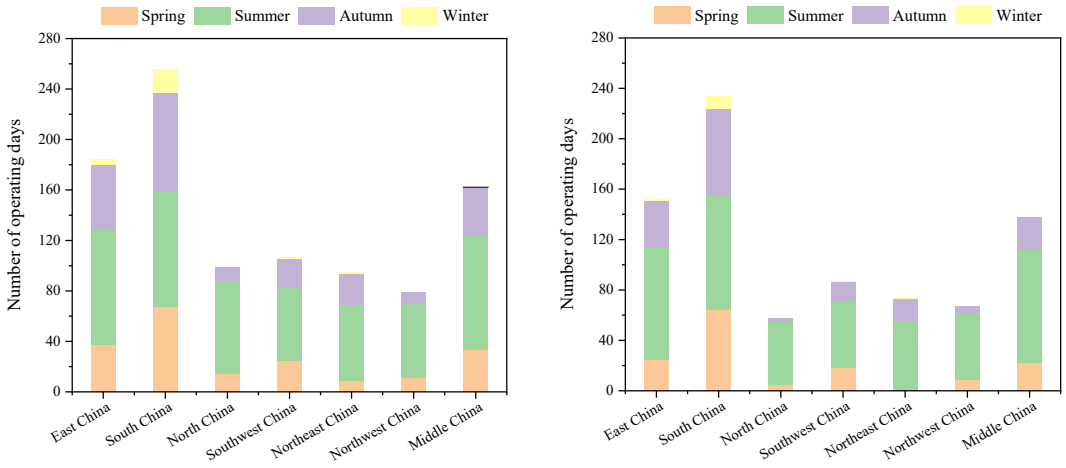

Fig. 8 Total number of the average operation days in a whole year. (a) Working period (b) Non-working period

In the beginning, the average number of operating days of seven geographic regions during the working and non-working periods in four seasons need to be mentioned. Then, the annual average temperature decrease, humidity drop, and cooling capacity IEC can be calculated based

on the operating days, while the days with no cooling load were not considered. As seen in Fig. 8, more operating days are counted from the working period. Among the seven geographic regions, South China holds the most extended operation durations of the AC system, namely 256 and 234 days, in both working and non-working periods. East China and middle China come to the second and third places, respectively. In addition, the shortest number of operating days is counted as 79 days in Northwest China for daytime, but it turns to north China as 58 days in the nighttime.

Combining the local weather conditions with the established IEC-ANN model in section 2.2, the temperature drops, humidity drops, and cooling capacities of the IEC are calculated and plotted from Figs. 9-11. It can be counted that the IEC can contribute to greater annual temperature drops of 3.6 ℃, 3.59 ℃, and 3.59 ℃ in south China, east China, and middle China, respectively. The humidity decrease and total cooling capacities are also higher in the three geographical areas. Hence, south China, east China, and middle China can be preliminarily selected as the better regions to use IEC for air treatment. In addition, the temperature drop and total cooling capacity are found to be stronger during the working time, while the humidity reduction (dehumidification) is more active in the nighttime. Take south China as an example, the IEC achieves the best performance there than the other six areas, which contributes to higher annual average temperature decrease of 3.6 ℃ and cooling capacity of 3.63 kW but a lower humidity reduction of 0.56 g/kg in the working period, compared with them of 2.67 ℃ and 3.15 kW but a greater humidity drop of 0.68 g/kg in the non-working span.

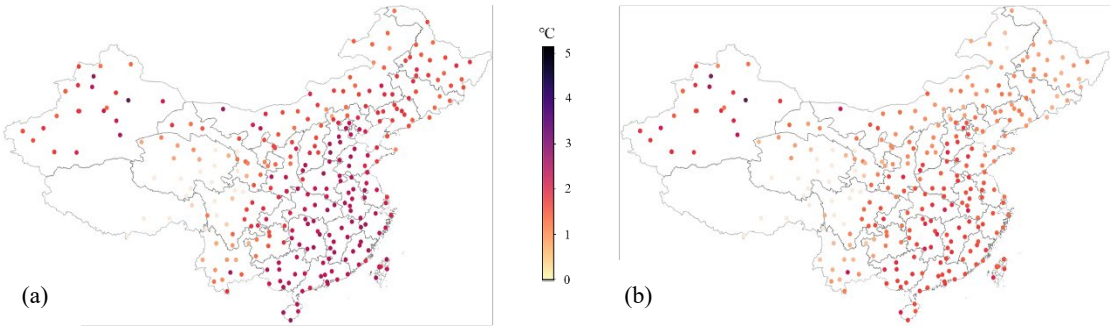

Fig. 9 Map of the IEC annually average temperature drop during (a) Working period (b) Non-working period

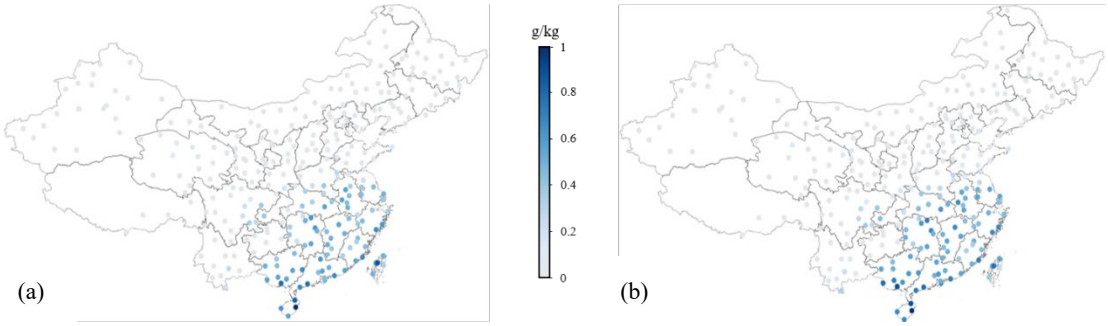

Fig. 10 Map of the IEC annually average humidity drop during (a) Working period (b) Non-working period

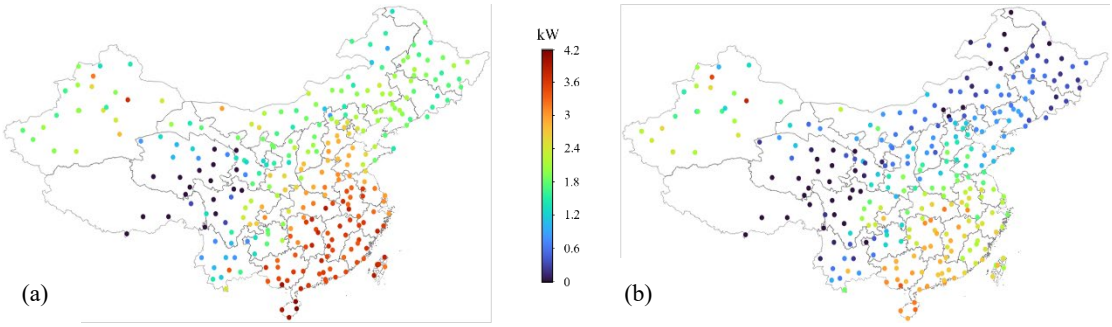

Fig. 11 Map of the IEC annually average total cooling capacity during (a) Working period (b) Non-working period

3.2 Seasonal average performance of IEC

Apart from illustrating the annual performance, the seasonal performance of IEC is necessary to be revealed. It needs to be mentioned that the days of winter are significantly fewer compared with the other three seasons, as seen from Fig. 8. Although air conditioning is required on several days in south China, there is almost no air cooling requirement in the other six regions. Therefore, the performance of IEC in winter is not discussed in this section. Analyses of the results from the IEC-ANN model based on the weather conditions of the operating days of spring, summer, and autumn were conducted in the seven geographical regions of China. In addition, we find that the distributions are similar during the daytime and nighttime. In order to make figures clear and concise, performance maps in the working period are decided as representatives for describing the tendencies, and the comparisons of the results between the two spans are given in the bar charts.

3.2.1 Temperature drop

In Fig. 12, the seasonal average temperature drops of IEC during the daytime in the three seasons are plotted on the map of China. The average values categorized by the seven geographic areas are shown in Fig. 13. There are more dark points that can be noticed in summer than spring and autumn for most regions, especially in south China, east China, and middle China. The average temperature drop of them are 4.52 ℃, 4.51 ℃, and 4.45 ℃ during the working time, and are 3.26 ℃, 2.87 ℃, and 3.09 ℃ in the nighttime, respectively, which consistently rank the top three out of seven. Specifically, the IEC can get a better air cooling effect in Hainan and Guangdong Provinces of south China, and so do Jiangxi Provinces, Taiwan Provinces, Fujian Provinces of East China, and Hunan Province of middle China. However, southwest China is observed to frequently include the points in light colors that indicate the less cooling performance, which achieves only 1.92 ℃ and 1.37 ℃ air temperature reduction in the two spans and comes to the last place of all.

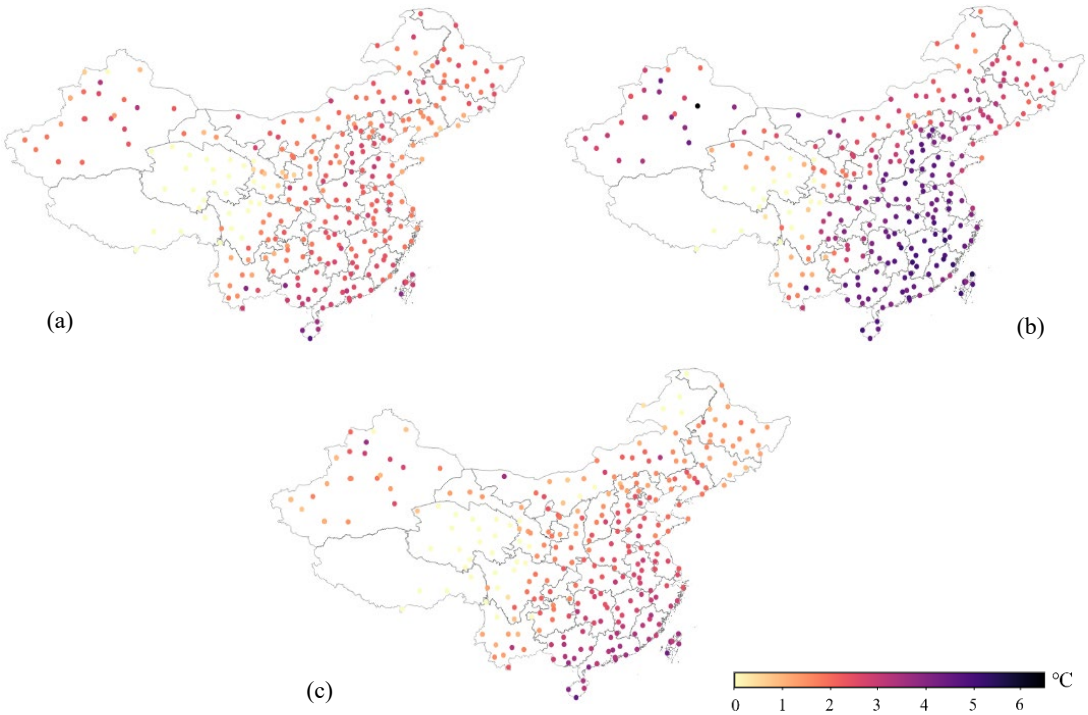

Fig. 12 Maps of the IEC seasonal average temperature drop during the working period. (a) Spring (b) Summer (c) Autumn

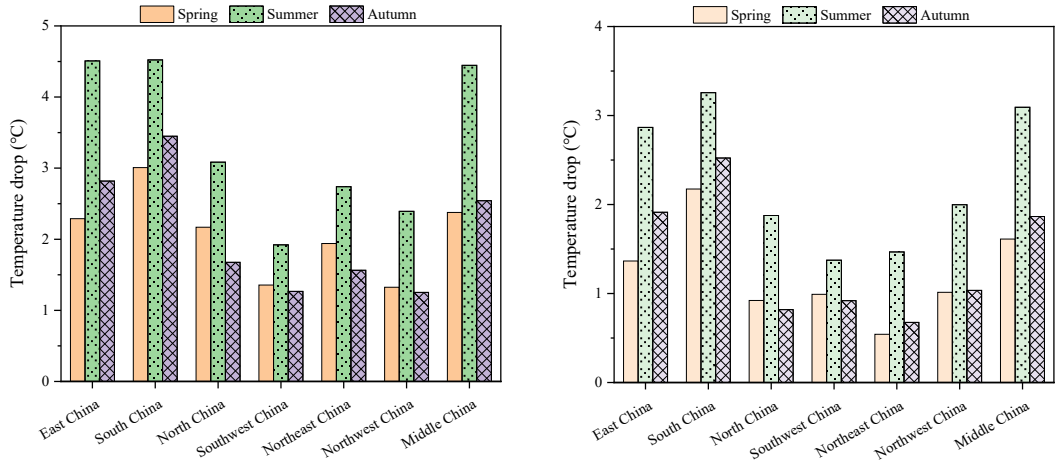

(a) (b)

Fig. 13 Summary of the average temperature drop by IEC in the seven geographic regions of China. (a) Working period (b) Non-working period

3.2.2 Humidity drop

Fig. 14 exhibits the humidity drops (dehumidification) contributed by IEC in the three seasons on the map of China. The average geographical humidity differences are summarized in Fig. 15. It should be noted that the feature of humidity removal is only produced when the IEC uses the cool secondary air source such as the exhaust air from indoor air-conditioned areas. If both the primary air and the secondary air are the fresh outdoor air, the lowest temperature

that the primary air can be cooled is the wet-bulb temperature of the secondary air. Nonetheless, when extracting the cool indoor air into the secondary air channel, if the wet-bulb temperature of the cool air is lower than the dew-point temperature of the primary air, dehumidification of the primary air becomes feasible.

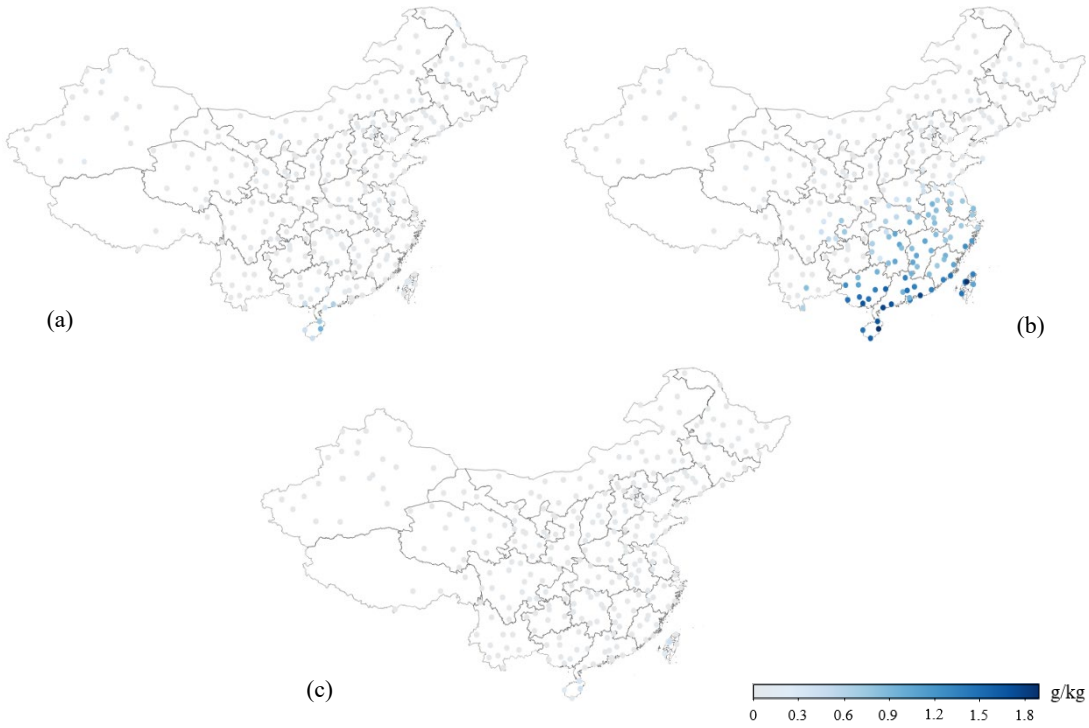

Fig. 14 Map of the IEC seasonal average humidity drop in (a) Spring (b) Summer (c) Autumn

Regarding the performance, Fig. 14(b) shows that the climate of south China and east China makes IEC more favorable for handling latent heat of outdoor air. Specifically, for example, Hainan Province and Taiwan Province have the humidity differences of 1.61 g/kg and 1.42 g/kg, which rank the first and second places among all Provinces. Besides, other regions with good humidity reduction are Guangdong Province and Guangxi Province in south China, and Fujian Province and Zhejiang Province in east China. It can be noted from Fig. 15 that the humidity difference mainly happens in some regions in summer, and the average values at night are slightly higher than that during the daytime. However, no matter whether it is during the working or rest period of spring, the dehumidification of the IEC is limited in most areas except in south China and Taiwan Province in East China, and the average value is less than 0.1 g/kg. Furthermore, the humidity drop becomes even more subtle in autumn, which is approximately zero.

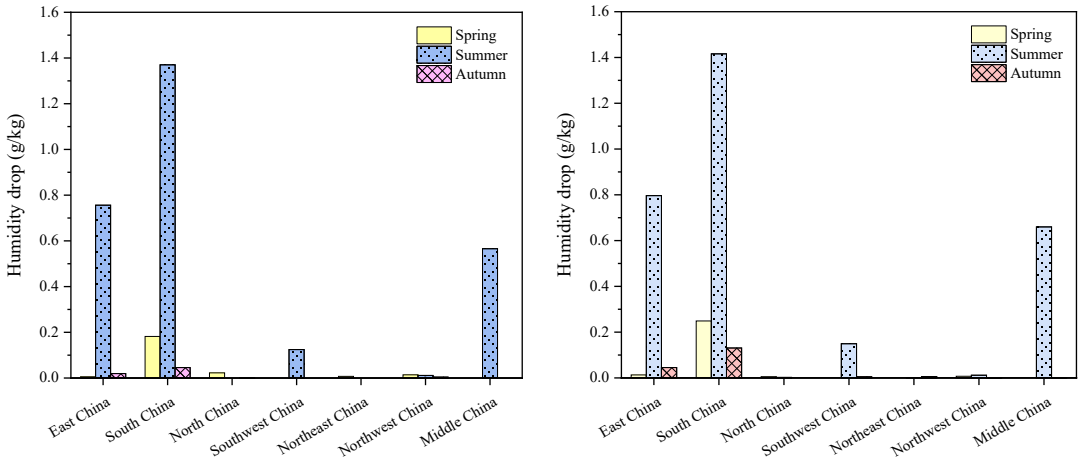

Fig. 15 Summary of the average humidity drop by IEC in the seven geographic regions of China. (a) Working period (b) Non-working period

3.2.3 Cooling capacity

The seasonal total cooling capacities of the IEC in China are shown in Fig. 16. The average geographical cooling capacities are presented in Fig. 17. As the same trend of temperature and humidity drop in most regions, the IEC displays better cooling capacities in summer than in the other two seasons. In comparison with other regions, the strongest cooling capacity of IEC is realized in south China with an average value of 5.74 kW during the working period, which is significantly greater than that of 4.62 kW (the second place) in East China and 4.24 kW (the third place) in middle China. Therefore, the climate conditions of the cities in south China are suitable for IEC to give full scope to its overall air cooling capability. Specifically, the optimal cooling capacities of IEC are obtained in Hainan Province and Guangdong Province, which are 6.42 kW and 5.67 kW on average. Besides, Taiwan Province is another region with good results of 6.03 kW, ranking the first place among the areas of east China. However, the overall cooling capacity of IEC in Southwest China seems to be quite limited with only 1.95 kW even in summer, and it counts the last among all geographic regions.

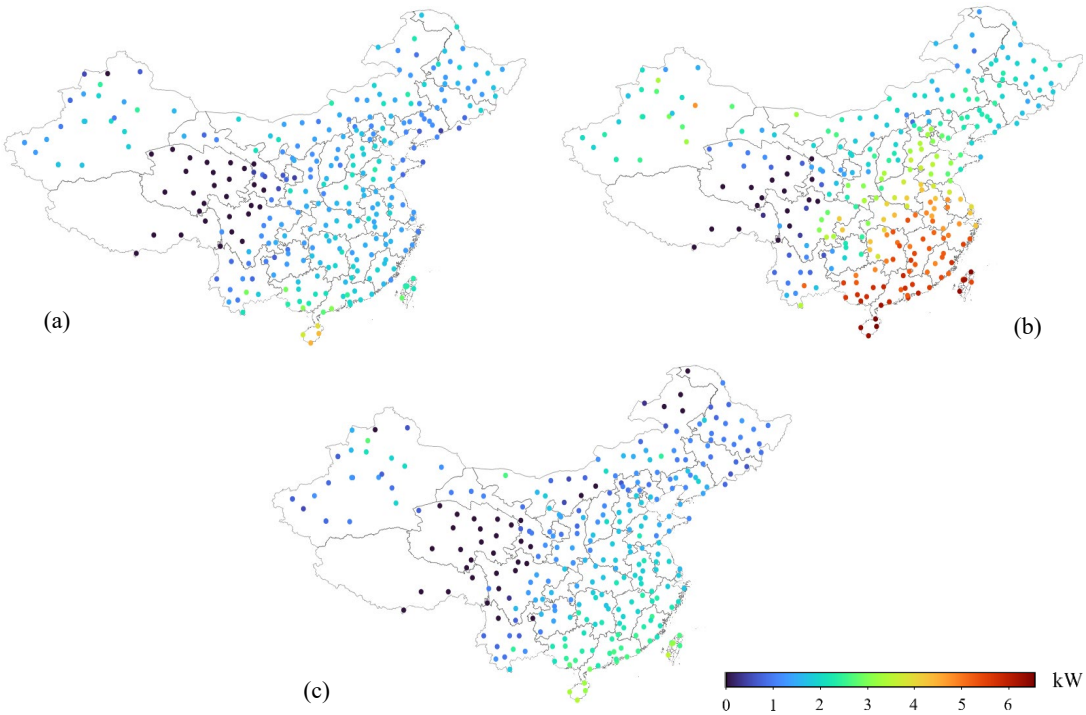

Fig. 16 Map of the IEC seasonal cooling capacity in (a) Spring (b) Summer (c) Autumn

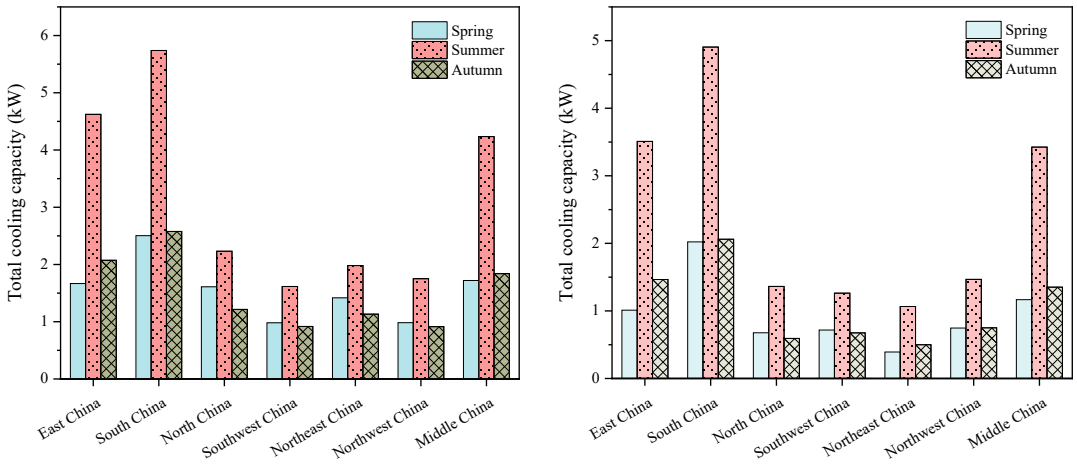

Fig. 17 Summary of the average cooling capacity by IEC in the seven geographic regions of China. (a) Working period (b) Non-working period

In addition, a detailed comparison of the cooling capacities in cities during the working and non-working periods was shown in Fig. 18. It can be seen that the cooling capacity during the working period is higher than that during the non-working period. Interestingly, the amounts of cooling capacity in the daytime are found to be 39.9% and 31.6% more than that of the nighttime in spring and autumn, but the percentage decreases to 24.5% in summer. This is because the IEC only treats the cooling load during the daytime in the spring and fall, but there is no load at night in some cities. Therefore, by adopting this IEC-ANN model for predictions,

the operation strategies of the IEC system in the rest period can be adjusted in some cities, such as closing the pumps and the secondary air fan in the IEC system to save operating energy. Under this circumstance, the IEC serves as ventilation equipment.

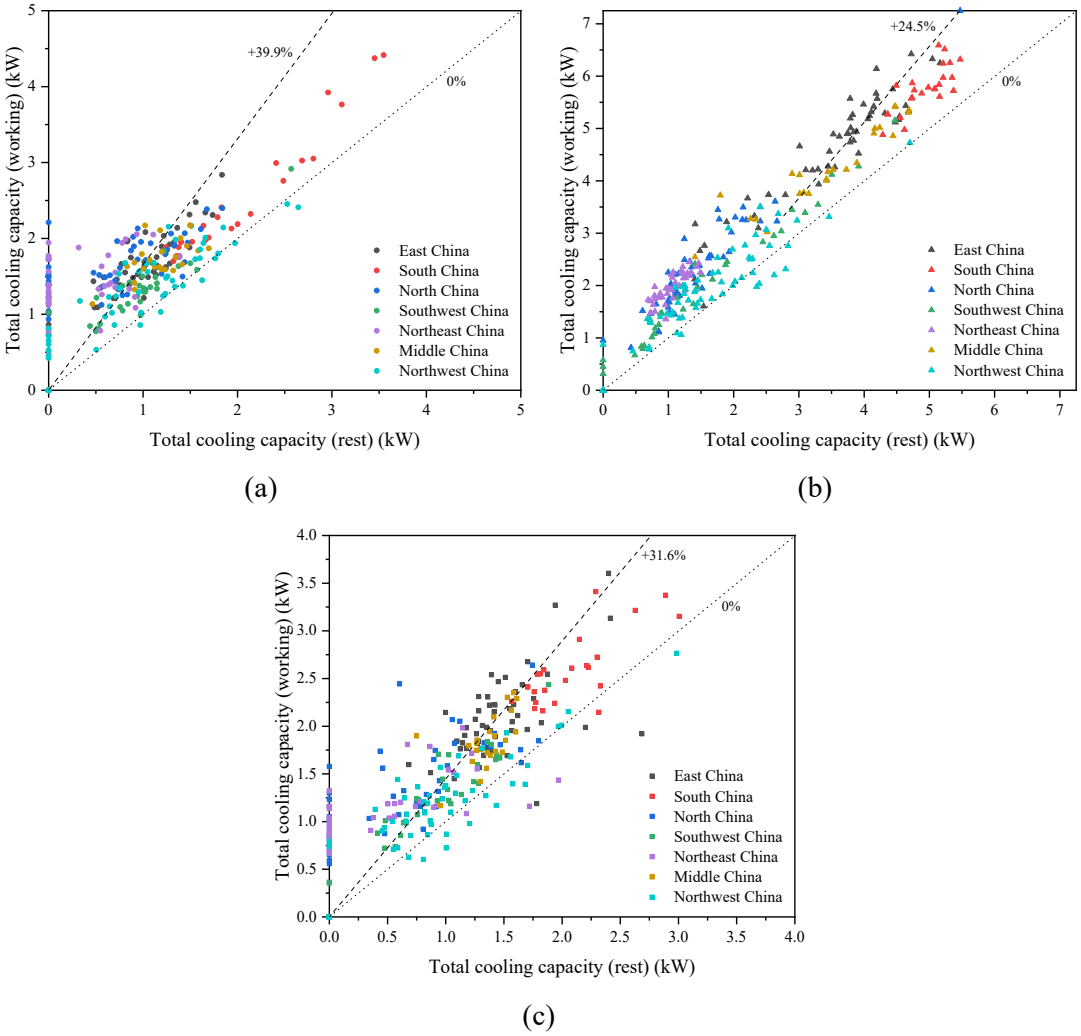

Fig. 18 Comparison of the cooling capacity during the working and non-working periods. (a) Spring (b) Summer (c) Autumn

3.3 Comparison of inference time between this IEC-ANN model and the numerical model

In addition to displaying the IEC performance maps of China and identifying the optimal application regions, the short inference time of this IEC-ANN model needs to be emphasized. An inference is the forward propagation process of getting an output when given an input [30]. The inference times of the ANN model and the numerical IEC model were counted and recorded. The calculations were executed using the regular personal computer of Intel(R) Core (TM) i7-10700F central processing unit (CPU) with 2.90 GHz and 16.0 GB of Random Access Memory (RAM). The test was conducted by inputting the same sets of variables into models. Because the internal mechanism of the computer is slightly different at every moment, the time consumed for calculation is not exactly the same in each test, but it will fluctuate stably within

a specific range. The time evaluation includes two parts. The first part was to test the time spent on calculating once. The second part examined the time consumed in working out groups of data in a week, and the cumulative time difference between the two models could be observed. Each part was repeated 50 times. The comparisons between the IEC-ANN model and the numerical model are presented in Table 3.

Table 3 Comparison between this IEC-ANN model and the numerical model

Type of the IEC model	IEC-ANN model	Numerical model
Inference time	4.4×10^{-4} ms (1) 0.03 ms (2)	2180 ms (2.18 s) (1) 152.6 s (2)
RMSE of temperature	0.328 ℃	0.488 ℃
RMSE of humidity	0.742 g/kg	0.637 g/kg

Notes:

1) The inference time consumed in calculating one group of data.

2) The inference time spent on processing groups of on-site measurement data from the project of section 2.3.2 in a week.

3) *RMSEs* are calculated based on the same groups of data mentioned in note (2).

It can be observed from Table 3 that the inference time of calculating once by this IEC-ANN model is significantly less than that of the numerical model with the close *RMSE* when given the same task. The IEC-ANN model only consumes 4.4×10^{-4} ms to finish a group of input data, while the numerical model needs 2.18 s, which is much longer than the former. Furthermore, this IEC-ANN model only takes around 0.03 ms to figure out the outlet air properties for a week, but the numerical model needs to consume 152.6 s for this same number of groups of input data. Therefore, it can be realized that the time difference between the two models increases rapidly with the growing quantities of input data. This reveals that the IEC-ANN model is conducive to improving work efficiency in the engineering stage owing to the much less inference time.

4. Limitation of this IEC-ANN model

The current IEC-ANN model can predict the cooling performance at an extremely short inference time. However, the limitation still can be recognized: This model is established based on the data of the normal plate-type cross flow IEC, so it can only predict the cooling performance of this type of IEC. In other words, this model cannot be applied to forecast the cooling effect of other types of IEC in different configurations or novel shapes such as the counter flow IEC [31], the tubular IEC [32], rotary IEC [33] or IECs with hexagon heat transfer sheet [3].

5. Conclusions

In this study, a model of a cross-flow indirect evaporative cooler using the cold exhaust air from an indoor air-conditioned area as secondary air source was proposed based on the artificial neural network (IEC-ANN), which was verified with the on-site measurement data from an engineering project. Combining with the outdoor weather conditions in different locations, the annual and seasonal maps of performances were presented for different locations in China during the working and non-working periods. The optimal regions to use the IEC to contribute better cooling effect were also identified. Furthermore, the comparison of the inference time was carried out between the IEC-ANN model and the numerical IEC model. The main results are summarized as follows.

1) All the annual average performances (temperature drop, humidity drop and cooling capacity) of an IEC in south China rank in first place among the seven geographical regions of China, which are 3.6 ℃, 0.68 g/kg and 3.63 kW, respectively. East China and middle China come to the second and third places, while the southwest comes to the last.

2) The seasonal average temperature drops and cooling capacities during the working period are more than those in the non-working period. South, east and middle China presents higher values again among the seven regions, which can be determined as the optimal regions to use the IEC for air cooling. The greatest average temperature drop and the strongest cooling capacity occur in south China, which are 4.52 ℃ and 5.74 kW, respectively.

3) The seasonal average humidity drops of the studied regions are stronger when the IEC operates during nighttime, but the maximum humidity differences are obtained as 1.61 g/kg and 1.42 g/kg in Hainan Province of south China and Taiwan Province of east China during the daytime period, respectively.

4) Given the same groups of data, the inference time of the IEC-ANN model is much less than that of the numerical model, and the time benefit of this model can increase noticeably with larger quantities of calculated cases, which is promising to improve the working efficiency when it is used in a practical project.

Appendix – Maps of seasonal temperature and relative humidity of China

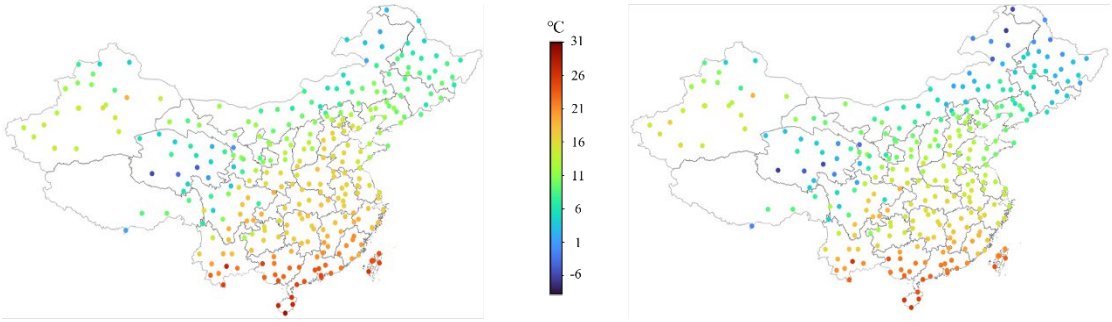

(a) Temperature

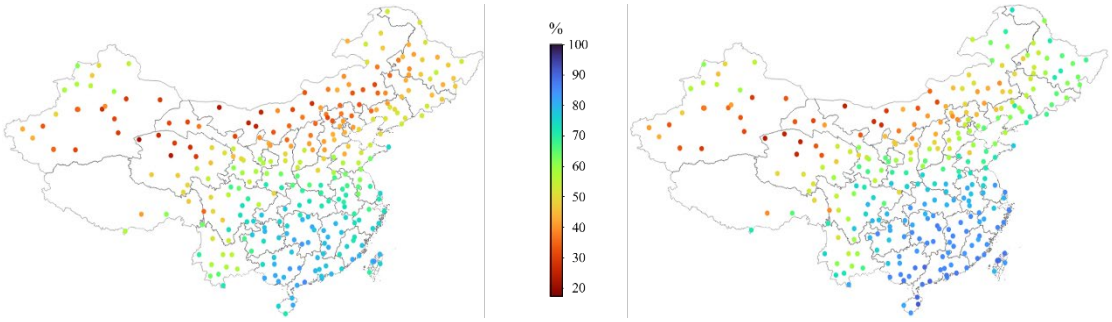

(b) Relative humidity

Fig. A1 Distributions of outdoor air conditions in spring (Left – working period; Right – non-working period)

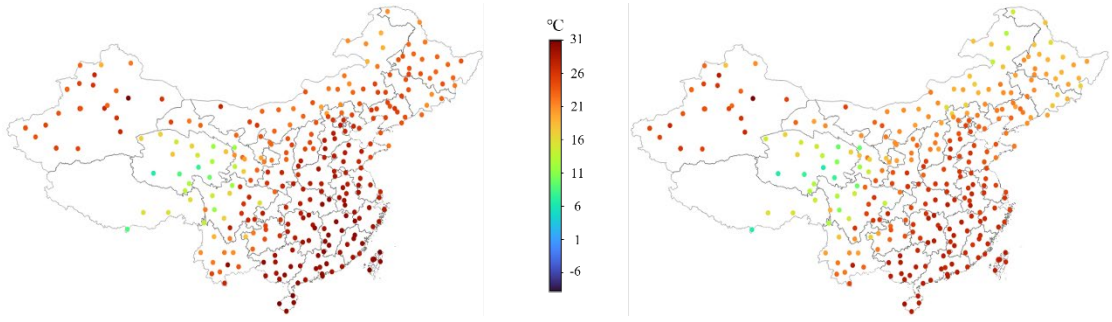

(a) Temperature

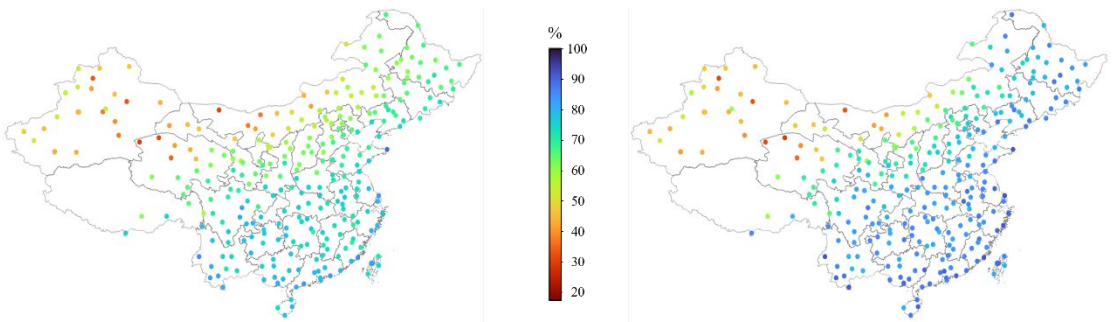

(b) Relative humidity

Fig. A2 Distributions of outdoor air conditions in summer (Left – working period; Right –

non-working period)

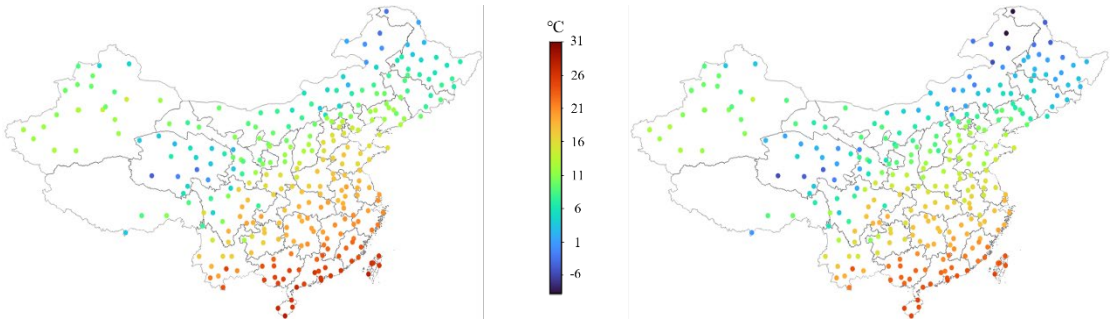

(a) Temperature

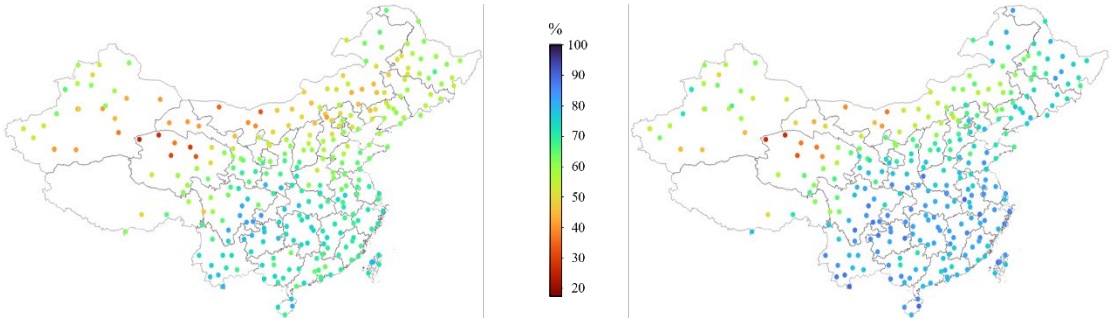

(b) Relative humidity

Fig. A3 Distributions of outdoor air conditions in autumn (Left – working period; Right – non-working period)

CRediT authorship contribution statement

Wenchao Shi: Conceptualization; Methodology; Program; Experiment; Writing – original draft. **Yunran Min:** Validation; Data curation; Formal analysis. Yu Gu: Validation; Program. **Xiaochen Ma:** Validation; Resources; Formal analysis. **Yi Chen:** Writing – review & editing. **Hongxing Yang:** Conceptualization; Supervision; Funding acquisition; Writing – review & editing.

Declaration of competing interest

The authors declare that they have no known competing financial interests or personal relationships that could have appeared to influence the work reported in this paper.

Acknowledgment

The authors wish to acknowledge the financial support provided by the General Research Fund projects of the Hong Kong Research Grant Council (Ref. No.: 15213219 and 15200420). Our appreciation also goes to the Electrical and Mechanical Services Department of the Hong Kong SAR Government for supporting the onsite tests of an IEC system.

References

[1] O. M. Zaki, R. H. Mohammed, and O. Abdelaziz, "Separate sensible and latent cooling technologies: A comprehensive review," *Energy Conversion and Management,* vol. 256, p. 115380, 2022/03/15/ 2022.

[2] R. Boukhanouf, A. Alharbi, H. G. Ibrahim, O. Amer, and M. Worall, "Computer modelling and experimental investigation of building integrated sub-wet bulb temperature evaporative cooling system," *Applied Thermal Engineering,* vol. 115, pp. 201-211, 2017/03/25/ 2017.

[3] L. Jia, J. Liu, C. Wang, X. Cao, and Z. Zhang, "Study of the thermal performance of a novel dew point evaporative cooler," *Applied Thermal Engineering,* vol. 160, p. 114069, 2019/09/01/ 2019.

[4] X. Cui, K. J. Chua, M. R. Islam, and K. C. Ng, "Performance evaluation of an indirect precooling evaporative heat exchanger operating in hot and humid climate," *Energy Conversion and Management,* vol. 102, pp. 140-150, 2015/09/15/ 2015.

[5] A. Adam, D. Han, W. He, and J. Chen, "Numerical analysis of cross-flow plate type indirect evaporative cooler: Modeling and parametric analysis," *Applied Thermal Engineering,* vol. 185, p. 116379, 2021/02/25/ 2021.

[6] Y. Wan, Z. Huang, A. Soh, X. Cui, and K. J. Chua, "Analysing the transport phenomena of novel dew-point evaporative coolers with different flow configurations considering condensation," *International Journal of Heat and Mass Transfer,* vol. 170, p. 120991, 2021/05/01/ 2021.

[7] W. Shi, Y. Min, Y. Chen, and H. Yang, "Development of a three-dimensional numerical model of indirect evaporative cooler incorporating with air dehumidification," *International Journal of Heat and Mass Transfer,* vol. 185, 2022.

[8] Y. Min, W. Shi, B. Shen, Y. Chen, and H. Yang, "Enhancing the cooling and dehumidification performance of indirect evaporative cooler by hydrophobic-coated primary air channels," *International Journal of Heat and Mass Transfer,* vol. 179, 2021.

[9] A. E. Kabeel and M. Abdelgaied, "Numerical and experimental investigation of a novel configuration of indirect evaporative cooler with internal baffles," *Energy Conversion and Management,* vol. 126, pp. 526-536, 2016/10/15/ 2016.

[10] W. Shi, Y. Min, X. Ma, Y. Chen, and H. Yang, "Dynamic performance evaluation of porous indirect evaporative cooling system with intermittent spraying strategies," *Applied Energy,* vol. 311, 2022.

[11] W. Shi, Y. Min, X. Ma, Y. Chen, and H. Yang, "Performance evaluation of a novel plate-type porous indirect evaporative cooling system: An experimental study," *Journal of Building Engineering,* vol. 48, 2022.

[12] Y. Chen, X. Huang, T. Sun, and J. Chu, "Experimental study of plant fiber-polymer composite for indirect evaporative cooler application," *Applied Thermal Engineering,* vol. 199, p. 117543, 2021/11/25/ 2021.

[13] D. B. Jani, M. Mishra, and P. K. Sahoo, "Performance prediction of rotary solid desiccant dehumidifier in hybrid air-conditioning system using artificial neural network," *Applied Thermal Engineering,* vol. 98, pp. 1091-1103, 2016.

[14] G. Zhu, T.-T. Chow, and C. K. Lee, "Performance analysis of counter-flow regenerative heat and mass exchanger for indirect evaporative cooling based on data-driven model," *Energy and Buildings,* vol. 155, pp. 503-512, 2017.

[15] S. Li *et al.*, "Zero energy potential of photovoltaic direct-driven air conditioners with considering the load flexibility of air conditioners," *Applied Energy,* vol. 304, 2021.

[16] Sholahudin, K. Ohno, N. Giannetti, S. Yamaguchi, and K. Saito, "Dynamic modeling of room temperature and thermodynamic efficiency for direct expansion air conditioning systems using Bayesian neural network," *Applied Thermal Engineering,* vol. 158, 2019.

[17] H. Wang, W. Cai, and Y. Wang, "Modeling of a hybrid ejector air conditioning system using artificial neural networks," *Energy Conversion and Management,* vol. 127, pp. 11-24, 2016.

[18] A. T. Mohammad, S. B. Mat, M. Y. Sulaiman, K. Sopian, and A. A. Al-abidi, "Artificial neural network analysis of liquid desiccant regenerator performance in a solar hybrid air-conditioning system," *Sustainable Energy Technologies and Assessments,* vol. 4, pp. 11-19, 2013.

[19] X. Xu, J. Liu, Y. Wang, J. Xu, and J. Bao, "Performance evaluation of ground source heat pump using linear and nonlinear regressions and artificial neural networks," *Applied Thermal Engineering,* vol. 180, 2020.

[20] Y. Min, Y. Chen, and H. Yang, "Numerical study on indirect evaporative coolers considering condensation: A thorough comparison between cross flow and counter flow," *International Journal of Heat and Mass Transfer,* vol. 131, pp. 472-486, 2019.

[21] Y. Chen, H. Yang, and Y. Luo, "Indirect evaporative cooler considering condensation from primary air: Model development and parameter analysis," *Building and Environment,* vol. 95, pp. 330-345, 2016.

[22] H. Yang, W. Shi, Y. Chen, and Y. Min, "Research development of indirect evaporative cooling technology: An updated review," *Renewable and Sustainable Energy Reviews,* vol. 145, 2021.

[23] Sholahudin *et al.*, "Experimental implementation of artificial neural network for cost effective and non-intrusive performance estimation of air conditioning systems," *Applied Thermal Engineering,* vol. 181, 2020.

[24] M. Barthwal and D. Rakshit, "Artificial neural network coupled building-integrated photovoltaic thermal system for indian montane climate," *Energy Conversion and Management,* vol. 244, p. 114488, 2021/09/15/ 2021.

[25] D. Graupe, *Principles of artificial neural networks*. World Scientific, 2013.

[26] A. A. Alnaqi, H. Moayedi, A. Shahsavar, and T. K. Nguyen, "Prediction of energetic performance of a building integrated photovoltaic/thermal system thorough artificial neural network and hybrid particle swarm optimization models," *Energy Conversion and Management,* vol. 183, pp. 137-148, 2019/03/01/ 2019.

[27] Y. Min, Y. Chen, W. Shi, and H. Yang, "Applicability of indirect evaporative cooler for energy recovery in hot and humid areas: Comparison with heat recovery wheel," *Applied Energy,* vol. 287, 2021.

[28] EnergyPlus. (2005, 15 March 2022). *Chinese Standard Weather Data* [Online]. Available: https://energyplus.net/weather.

[29] J. Chen, L. Lu, and Q. Gong, "A new study on passive radiative sky cooling resource maps of China," *Energy Conversion and Management,* vol. 237, p. 114132, 2021/06/01/ 2021.

[30] A. Discovery. (2021, 4 March). *How to Optimize a Deep Learning Model for faster Inference?* [Online]. Available: https://www.thinkautonomous.ai/blog/?p=deep-learning-optimization.

[31] J. Lin, K. Thu, T. D. Bui, R. Z. Wang, K. C. Ng, and K. J. Chua, "Study on dew point evaporative cooling system with counter-flow configuration," *Energy Conversion and Management,* vol. 109, pp. 153-165, 2016/02/01/ 2016.

[32] T. Sun, X. Huang, Y. Qu, F. Wang, and Y. Chen, "Theoretical and experimental study on heat and mass transfer of a porous ceramic tube type indirect evaporative cooler," *Applied Thermal Engineering,* vol. 173, p. 115211, 2020/06/05/ 2020.

[33] D. Pandelidis *et al.*, "Performance analysis of rotary indirect evaporative air coolers," *Energy Conversion and Management,* vol. 244, p. 114514, 2021/09/15/ 2021.